SPANDIDOS PUBLICATIONS

INTERNATIONAL JOURNAL OF ONCOLOGY 60: 47, 2022

Spine-specific downregulation of LAPTM5 expression promotes the progression and spinal metastasis of estrogen receptor-positive breast cancer by activating glutamine-dependent mTOR signaling

QINGBING MENG[1-3], LEI ZHOU[1,2], HAIFENG LIANG[1,2], ANNAN HU[1,2], HAO ZHOU[4], JIAN ZHOU[1,2], XIAOGANG ZHOU[1,2], HONG LIN[1,2], XILEI LI[1,2], LIBO JIANG[1,2] and JIAN DONG[1,2]

[1]Department of Orthopaedic Surgery, [2]Cancer Center, Zhongshan Hospital, Fudan University, Shanghai 200032; [3]Human Phenome Institute, Fudan University, Shanghai 201203; [4]Department of Orthopedic Surgery, Xuhui-Zhongshan Hospital, Fudan University, Shanghai 200032, P.R. China

Received November 3, 2021; Accepted January 24, 2022

DOI: 10.3892/ijo.2022.5337

Abstract. Estrogen receptor-positive (ER^+) breast cancer (BC) is a malignancy that is prone to metastasis to the spine, which is difficult to treat and often results in poor prognosis. However, the mechanism underlying the tumorigenesis and spinal metastasis of ER^+ BC remains unclear. Lysosomal protein transmembrane 5 (LAPTM5) has been reported as a tumor suppressor in several types of cancer, but its role in ER^+ BC has not been described. Here, by analyzing a gene sequencing dataset and ER^+ BC tissues, tumor-adjacent normal tissues and spinal metastatic tissues from patients and mouse models, we found that LAPTM5 expression is negatively related to the progression and spinal metastasis of ER^+ BC. Subsequently, *in vitro* experiments demonstrated that downregulation of LAPTM5 expression promoted the proliferation, migration, and chemoresistance of ER^+ BC cells by activating glutamine-dependent mTOR signaling. A high level of CX3CL1 could inhibit LAPTM5 expression, explaining how ER^+ BC metastasized to the spine. Thus, we found that LAPTM5 functions as a tumor suppressor in ER^+ BC and that the CX3CL/CX3CR1/LAPTM5/glutamine axis mediates the spinal metastasis of ER^+ BC. This axis may be a promising therapeutic target for ER^+ BC.

Introduction

Breast cancer (BC) has one of the highest incidences of all malignant tumors worldwide and has the highest mortality rate in females (1). Specifically, in China, 270,000 patients were diagnosed with BC and 70,000 BC patients died from the disease in 2015 (2). BC has been reported as the most common type of malignancy that is likely to metastasize to bone, with a high prevalence of 70 to 90% in patients with known primary BC in a study of postmortem cadavers (3,4). Moreover, the prolonged survival of BC patients due to advances in diagnosis and treatment has led to an increased rate of metastasis (5). Approximately 65% of advanced BC patients develop bone metastasis (6). Among them, 80% of BC bone metastases are located in the spine; 70 to 80% of BC is the estrogen receptor-positive (ER^+) subtype, and luminal subtypes (ER^+) of BC are reported to be highly associated with bone metastasis (7,8). Therefore, spinal metastasis (SM) of ER^+ BC is common among bone metastatic tumors, which is consistent with our clinical experience. As the late stage of ER^+ BC, SM is highly malignant and always resistant to chemotherapies (7,8). However, few studies have focused on the SM of BC, and the potential mechanism underlying the progression and SM of ER^+ BC remains unclear.

We screened relevant genes involved in the SM of ER^+ BC and identified lysosomal protein transmembrane 5 (LAPTM5) as an SM-related gene. As a protein located in the lysosomal membrane, LAPTM5 is thought to be preferentially expressed in immune cells (9-11). However, recent studies have reported that LAPTM5 expression is downregulated in various types of cancers, including lung cancer, esophageal squamous cell carcinoma, and glioblastoma, indicating that the tumor-suppressive function of LAPTM5 and downregulated expression of this gene may play a role in tumor progression (12,13). However, the exact role of LAPTM5 in human BC remains unknown.

Cancer cells are characterized by their reprogrammed nutrient metabolism (14,15). Recently, glutamine was reported to be one of the key nutrients of BC, and glutamine metabolism facilitates the proliferation, progression and chemoresistance of BC (16,17). During the process of glutamine metabolism, sodium-dependent neutral amino acid transporter type 2 (SLC1A5) and glutaminase 1 (GLS1) are two critical molecules. The former mediates uptake of neutral amino acids including glutamine, and the latter catalyzes glutamine into glutamate (18,19). Gene set enrichment

Correspondence to: Professor Jian Dong, Department of Orthopaedic Surgery, Zhongshan Hospital, Fudan University, 180 Feng Lin Road, Xuhui, Shanghai 200032, P.R. China
E-mail: dong.jian@zs-hospital.sh.cn

Key words: estrogen receptor-positive breast cancer, spinal metastasis, LAPTM5, glutamine, mTOR, CX3CL1/CX3CR1

analysis has indicated that LAPTM5 expression is related to the nutrient metabolism of ER+ BC. Moreover, some studies have shown that glutamine metabolism can activate mammalian target of rapamycin (mTOR), which plays an important role in regulating the fundamental physiological functions of cancer cells, including protein synthesis, proliferation, migration, and autophagy (20,21). Therefore, we speculated that glutamine-dependent activation of mTOR signaling may mediate the biological function of LAPTM5.

C-X3-C motif chemokine ligand 1 (CX3CL1) has been regarded as an essential mediator in tumor metastasis via binding to its receptor CX3CR1-expressing cells to endothelial cells (22). Our previous research and other works confirmed that CX3CL1/CX3CR1 interaction is involved in the survival, adhesion, and migration of breast cancer cells (23,24). Furthermore, a higher level of CX3CL1/CX3CR1 was found in vertebrae than in limb bone, which may account for SM (23,25). However, the exact molecular mechanism of CX3CL1/CX3CR1-mediated SM of breast cancer still remains unclear.

Collectively, we hypothesized that downregulation of LAPTM5 expression could enhance the progression of ER+ BC by activating glutamine-dependent mTOR signaling. To examine our hypothesis, we detected the impact of LAPTM5 expression on glutamine metabolism and activation of downstream mTOR signaling in ER+ BC both *in vitro* and *in vivo*. Subsequently, we explored the role of LAPTM5 in the SM of ER+ BC using a mouse model of SM. The aims of this study were to ascertain the role of LAPTM5 in tumorigenesis and the SM of ER+ BC and reveal the underlying mechanism.

Materials and methods

ER+ BC specimens. A total of 19 clinical specimens were obtained from the Department of Orthopedic Surgery, Zhongshan Hospital, Fudan University and the Department of General Surgery, Xuhui-Zhongshan Hospital, Fudan University. The specimens included 7 SM samples of ER+ BC (median age, 53 years; range, 43-60 years), 6 samples of primary ER+ BC (median age, 49.5 years; range, 45-60 years), and 6 corresponding tumor-adjacent normal tissues of primary ER+ BC. The clinicopathological data of these patients are shown in Table SI. The acquisition of patient specimens and the research procedures were approved (approval no. Y2019-085, 2019.02.27) by the Ethics Committee of Zhongshan Hospital, Fudan University. The relevant rules and regulations of the Ethics Committee of Zhongshan Hospital, Fudan University were strictly followed, and informed consent was provided by all patients.

Bioinformatics analysis. Gene Ontology (GO; http://geneontology.org/) and Kyoto Encyclopedia of Genes and Genomes (KEGG; https://www.kegg.jp/kegg/) analyses were used to identify the biological functions of LAPTM5 expression in ER+ BC. The biological processes and enriched pathways of the proteins encoded by the candidate genes were analyzed using The Database for Annotation, Visualization and Integrated Discovery (DAVID 6.8, https://david.ncifcrf.gov/home.jsp) (26,27). P<0.05 was set as the cut-off criterion. The GEO2R web tool (ncbi.nlm.nih.gov/geo/geo2r/) was used to analyze the gene expression profile of LAPTM5 in ER+ BC tissues from patients with primary disease or SM (GSE14661) (28). Gene Set Enrichment Analysis (GSEA; https://www.gsea-msigdb.org/gsea/index.jsp) was performed to screen the GO terms and KEGG pathways that may be associated with LAPTM5 in the database.

Cell lines. 293T cells (SCSP-502) and the human ER+ BC cell lines MCF-7 (SCSP-531) and T47D (KG115) were purchased from The Cell Bank of Type Culture Collection of the Chinese Academy of Sciences. The above cells were maintained in Dulbecco's modified Eagle's medium (DMEM, Gibco/Thermo Fisher Scientific, Inc.) containing 10% fetal bovine serum (FBS, 10091-148, Gibco/Thermo Fisher Scientific, Inc.) with incubation in humidified air containing 5% CO_2 at 37˚C.

Reagents. The glutaminase inhibitor BPTES (S7753), the CX3CR1 inhibitor JMS-17-2 (S0135), the AKT inhibitor MK-2206 (S1078), and docetaxel (S1148) were purchased from Selleck Chemicals (China). Lipofectamine® 3000 was purchased from Invitrogen (L3000001; Thermo Fisher Scientific, Inc.). Recombinant human fractalkine/CX3CL1 was purchased from MedChemExpress (HY-P7355, China).

Plasmids and lentivirus. The third-generation lentivirus packing system including hU6-MCS-ubiquitin-EGFP-RES-puromycin, psPAX2, and pMD2.G was purchased from GeneChem (China). Three RNAi sequences targeting human *LAPTM5* were designed (*LAPTM5* shRNA1, gcGGTGCTACAGATTGATCAA; shRNA2, tcATAACCAGTTCATCAAGAT; and shRNA3, gcTCCAGGAAATAACAGTTAT). Then, the three shRNAs targeting human *LAPTM5* were designed, annealed, and inserted into the lentivirus. For ER+ BC cell lines that stably overexpressed LAPTM5, the lentivirus plasmid GV657-LAPTM5 was constructed by subcloning the LAPTM5 coding sequence (Gene ID: 7805) into the modified GV657-puro backbone (GeneChem, China). The abovementioned plasmids (7 μg psPAX2, 3 μg pMD2.G, 1 μg shRNA) were added to 293T cells at approximately 30% density with 20 μl of Lipofectamine 3000 (L3000-015; Invitrogen/Thermo Fisher Scientific, Inc.). After incubation for 6 to 12 h, the culture medium was changed to fresh DMEM containing 10% FBS. Culture medium containing the lentivirus was collected at 2 and 3 days, filtered through a 0.45-μm cellulose acetate filter (Millipore) and stored in an ultra-low temperature refrigerator. MCF-7 and T47D cells were infected by the lentivirus with 6 μg/ml polybrene (TR-1003; Sigma-Aldrich/Merck KGaA) for 72 h at 37˚C. Finally, the successfully transfected cells were screened out using puromycin (A1113802; Thermo Fisher Scientific, Inc.) for 1 week.

Colony formation assay. ER+ BC cells in a logarithmic growth state were digested with 0.25% trypsin and blown into single cells. The cells were suspended in the culture medium and inoculated in a culture dish at 500 cells/well. The cells were incubated at 37˚C with 5% CO_2 and saturated humidity for 2 to 3 weeks. When obvious clones appeared in the culture dish, the experiment was terminated. The supernatant was discarded, and the cells were washed twice with PBS buffer. Five milliliters of 4% paraformaldehyde was added to fix

the cells for 15 min. Then, the fixing solution was removed, and 1% crystal violet was added to dye for 10 min. After the dyeing solution was washed away with running water, the clones could be counted with the naked eye and photographed (E-M10 MarkIV; Olympus).

Wound healing assay. ER^+ BC cells were seeded in 6-well plates at a density of $1x10^5$ cells per well and cultured to approximately 90% confluence. A horizontal wound was created and photographed immediately. The cells were then stimulated with 2 μM docetaxel or control PBS buffer. Finally, the images at 24 and 48 h were also captured (CKX53; Olympus), and the wound areas after healing were measured and calculated.

Cell inhibition assay. ER^+ BC cells were seeded in 96-well culture plates (3,000 cells/well) and cultured at 37˚C with 5% CO_2. For growth inhibition assays, after incubation for 12 h for cell adherence to culture plates, a concentration gradient of docetaxel or control PBS buffer was added for 72 h of incubation at 37˚C. Then, 10 μl/well of Cell Counting Kit (CCK-8, CK04; Dojindo, Japan) reagent was added after an additional 2 h incubation at 37˚C. Finally, the optical density (OD)450 value was detected by a microplate reader, and the half maximal inhibitory concentration (IC_{50}) was calculated by GraphPad Prism 8 software (GraphPad Software, Inc.).

Western blot analysis. Protein samples were extracted from tissues or cells by RIPA lysis buffer (P0013B; Beyotime Institute of Biotechnology) containing phenylmethanesulfonyl fluoride (ST505, Beyotime Institute of Biotechnology) and phosphorylase inhibitor (78445; Thermo Fisher Scientific, Inc.). The protein concentration was determined with a Pierce™ BCA protein quantification kit (23225; Thermo Fisher Scientific, Inc.). Twenty micrograms of protein sample was separated by 10% SDS-PAGE, transferred to a PVDF membrane (ISEQ00010; Millipore), and blocked using 5% fat-free milk for 1 h at 25˚C. Then, the membranes were incubated with primary antibodies against LAPTM5 (PA5-23585; Thermo Fisher Scientific, Inc., 1:1,000), SLC1A5 [8057; Cell Signaling Technology, Inc. (CST), 1:1,000], GLS1 (56750, CST, 1:1,000), glutaminase 1 (GLS2) (ab150474; Abcam, 1:1,000), Raptor (48648, CST, 1:1,000), ribosomal protein S6 kinase 1 (S6K1) (14130, CST, 1:1,000), phosphorylated (p-) S6K1 (9209, CST, 1:1,000), eukaryotic translation initiation factor 4E (eIF4E)-binding protein 1 (4EBP1) (9644, CST, 1:1,000), p-4EBP1 (2855, CST, 1:1,000), matrix metallopeptidase 9 (MMP9) (13667, CST, 1:1,000), cyclin D1 (55506, CST, 1:1,000), NFκB p65 (8242, CST, 1:1,000), NFκB p-p65 (3033, CST, 1:1,000), Histone H3 (4499, CST, 1:1,000), PI3K (4249, CST, 1:1,000), p-PI3K (13857, CST, 1:1,000), AKT (4691, CST, 1:1,000), p-AKT Ser473 (4060, CST, 1:1,000), p-AKT Thr308 (13038, CST, 1:1,000), and β-actin (3700, CST, 1:1,000) at 4˚C overnight and incubated with anti-mouse (43593, CST, 1:3,000) or anti-rabbit secondary antibodies (7074, CST, 1:3,000) for 2 h at 25˚C. Proteins were visualized using Pierce™ ECL western substrate (32209; Thermo Fisher Scientific, Inc.). Quantitative analysis of relative protein expression was performed with ImageJ software (1.52 V; National Institutes of Health).

Real time-quantitative PCR (qPCR). Total RNA of tissues or cultured cells was extracted by TRIzol reagent (15596026; Invitrogen/Thermo Fisher Scientific, Inc.). Then, the PrimeScript™ RT reagent Kit (RR037Q; Takara) was applied for reverse transcription. Real-time PCR was conducted using TB Green® Fast qPCR Mix according to the manufacturer's instructions (RR430S; Takara) using a thermocycler (Thermo-ABI 7500; Thermo Fisher Scientific, Inc.). The primers used in this experiment were purchased from Sangon Biotech (China) and were as follows: LAPTM5: forward, 5'-GCGTCTTGTTGTTCATCGAGC-3'; reverse, 5'-CGATCC TGAGGTAGCCCAT-3'; GAPDH: forward, 5'-GGAGCG AGATCCCTCCAAAAT-3'; reverse, 5'-GGCTGTTGTCAT ACTTCTCATGG-3'. The following thermocycling conditions were used: initial denaturation at 95˚C for 30 sec followed by 35 cycles at 95˚C for 5 sec and 60˚C for 30 sec. The $2^{-\Delta\Delta Cq}$ method was used for relative quantification of the genes, and GAPDH was used as the internal reference (29).

Animal experiments. Male nude mice aged 4-6 weeks (weight, 15-17 g) were obtained from Vital River Laboratory Animal Technology (China) and randomly assigned to experimental groups. The animals were housed under controlled environmental conditions (12 h dark/light cycle; 20-22˚C; humidity, 55±5%), and allowed free access to normal food and water. A total of 15 mice (five in each group) were anesthetized by intraperitoneal injection of 0.3% sodium pentobarbital (30-60 mg/kg). For the *in vivo* subcutaneous tumorigenesis assay, $2x10^6$ blank, LAPTM5-sh3, and LAPTM5-OE MCF-7 cells were injected into the subcutaneous right forelimb armpit of the anesthetized mice. Then, 30 mg/kg docetaxel was injected via the tail vein once every other day. Tumor size was measured twice a week using a caliper to measure two perpendicular tumor diameters. Tumor volume (mm^3) was calculated as follows: Volume=0.5 x length x $width^2$. One month later, the mice were sacrificed by intraperitoneal injection of sodium pentobarbital (200 mg/kg, death was verified by respiratory and cardiac arrest, and pupil dilation), and the tumors were photographed and subjected to hematoxylin and eosin (H&E) staining and immunohistochemistry (IHC) staining as previously described (25).

For the SM assay, $1x10^6$ blank or LAPTM5-sh3 MCF-7 cells were injected into the left cardiac ventricle of the anesthetized mice (five in each group) (25). Docetaxel (30 mg/kg) was intravenously injected once every other day; BPTES (12.5 mg/kg) was intraperitoneally injected every 3 days (30), and JMS-17-2 (10 nM) was added to the cell suspension 30 min before inoculation (31). The development of SM was monitored by bioluminescence imaging (BLI) once a week using a Xenogen IVIS 200 Imaging System (Xenogen, USA) for 6-8 weeks. Finally, the mice were sacrificed when obvious SM could be observed via BLI in the control group, and the tumors were scanned by micro-computed X-ray tomography (micro-CT) and subjected to H&E and IHC staining. Micro-CT is a non-destructive 3D X-ray imaging technique used to study micro-changes of bone structure. Spinal metastasis of ER^+ BC mainly manifests as osteolytic destruction pathologically; therefore, micro-CT could show cortical defect and bone tissue destruction in the metastatic lesions of the spine. For the convenience of readers, we marked cortical defects and bone

tissue destructions with red arrows in Fig. 7B. The animal experimental procedures were approved by the Animal Ethics Committee of Zhongshan Hospital, Fudan University (accession number: Y2021-322), and their care was in accordance with institutional guidelines. No mice died unexpectedly during the experiment.

Statistical analysis. All data are presented as the mean ± SD of at least three repeated experiments. One-way analysis of variance (ANOVA) or two-tailed Student's t-test using GraphPad Prism 8 software (GraphPad Software, Inc.) was applied to analyze differences among groups. A P-value of <0.05 was considered statistically significant (*P<0.05, **P<0.01, and ***P<0.001, as denoted in the figures/legends).

Results

The LAPTM5 level is substantially decreased in SM samples of ER+ BC. LAPTM5 has been reported as a tumor suppressor in many types of cancer, but its role in ER+ BC is still unclear. First, we analyzed the gene expression profile of ER+ BC tissues from patients with primary disease or SM using the GEO2R web tool (32). The results showed that LAPTM5 was one of the top genes with downregulated expression in SM samples compared with primary tumors, indicating that it was negatively related to tumor progression and involved in SM in ER+ BC (Figs. 1A and S1). To verify the above sequencing results, we collected primary ER+ BC samples and SM samples from patients undergoing surgery in our hospital. As shown in Fig. 1B and C, IHC staining demonstrated decreased expression of LAPTM5 in ER+ BC both in the primary site and SM compared with the tumor-adjacent normal tissues, but the lowest level was observed in the SM samples. Furthermore, we established orthotopic ER+ BC and SM mouse models to strengthen our findings. The IHC (Fig. 1D and E), western blot analysis (Fig. 1F and G), and qPCR (Fig. 1H) results revealed that LAPTM5 expression was reduced sequentially in tumor-adjacent normal tissues, primary ER+ BC, and SM. Consistent with the above findings, the differences between each group were statistically significant. Collectively, these results demonstrated that downregulation of LAPTM5 expression is correlated with the spinal metastasis of ER+ BC.

LAPTM5 expression is correlated with the proliferation, migration, chemoresistance, and tumorigenesis of ER+ BC. To further examine the role of LAPTM5 in ER+ BC, we established LAPTM5-knockdown (sh) and -overexpressing (OE) MCF-7 and T47D cell lines. As shown in Figs. 2A-C and S2A and B, the LAPTM5-sh3 groups had the lowest expression level of LAPTM5 and were chosen for the following experiments. We first observed the impact of LAPTM5 expression on the proliferation and migration of ER+ BC cells with or without treatment with the chemotherapeutic drug docetaxel. The colony formation results showed an obviously enhanced growth rate of the LAPTM5-sh3 cells and an impaired proliferative capacity of the LAPTM5-OE cells without docetaxel treatment (Figs. 2D and E, S2C and D). After treatment with docetaxel, the growth rate of the cells in all three groups was reduced, but the LAPTM5-sh3 cells exhibited significant resistance to docetaxel, as they still formed many clones. Similarly, in the wound healing assay, the LAPTM5-sh3 cells showed the highest healing rate among the cells in all groups, while the LAPTM5-OE cells almost lost their migratory ability (Figs. 2F and G, S2E and F). Moreover, although docetaxel treatment for 48 h caused varying degrees of inhibition of the healing rate, the LAPTM5-sh3 cells still exhibited stronger migratory ability than other groups. The above cell experiments demonstrated that LAPTM5 inhibits the *in vitro* proliferation and migration of ER+ BC cells but promote their chemosensitivity.

Then, an *in vivo* subcutaneous tumorigenesis assay was conducted. Fig. 2H-J showed stronger tumorigenic ability of the LAPTM5-sh3 ER+ BC cells compared with the blank or LAPTM5-OE MCF-7 cells when mice were injected with docetaxel. The results of the histopathological examinations are shown in Figs. 2K, S2G and H. H&E and Ki-67 staining indicated the state of cell proliferation of the LAPTM5-sh3 group, while H&E and TUNEL staining demonstrated obvious necrosis of the LAPTM5-OE group under docetaxel treatment. Taken together, these data demonstrated that LAPTM5 was negatively associated with the proliferation and migration *in vitro* and tumorigenesis *in vivo* of the ER+ breast cancer cells under docetaxel treatment.

LAPTM5 regulates the malignant progression of ER+ BC through glutamine-mediated mTOR signaling. Before investigating the molecular mechanism underlying the regulatory effect of LAPTM5 on ER+ BC, we detected the IC_{50} of docetaxel in blank, LAPTM5-sh3, and LAPTM5-OE MCF-7 cells. As shown in Fig. 3A-D, the IC_{50} value of the LAPTM5-sh3 group was significantly higher than the values of the other groups, while LAPTM5 overexpression promoted the chemosensitivity of cancer cells. Given that the gene set enrichment analysis indicated that LAPTM5 may regulate cell metabolism and that glutamine is one of the key nutrient sources and is crucial for the biological function of BC (Fig. S3), glutamine metabolism was tested to verify our speculation. As shown in Fig. 3E-G, the glutamine transporters SLC1A5 and GLS1 showed significant upregulated expression when LAPTM5 was inhibited, illustrating the effect of LAPTM5 on glutamine metabolism. In addition, no significant changes were found in the glutaminase 2 (GLS2) expression between LAPTM5-silenced and control ER+ BC cells (Fig. S4). In addition as shown in Fig. 3E-G, the mTOR complex 1 (mTORC1) component Raptor and its downstream factors ribosomal protein S6 kinase B1 (S6K1) and eukaryotic translation initiation factor 4E binding protein 1 (4EBP1) were found to be significantly activated in the LAPTM5-sh3 cells. After phosphorylation of S6K1 (p-S6K1) and 4EBP1 (p-4EBP1), matrix metallopeptidase 9 (MMP9), cyclin D1, and intranuclear and phosphorylated NFκB p65 (NFκB p-p65) were subsequently activated, explaining the enhanced migration, proliferation and chemoresistance of LAPTM5-sh3 cells. In contrast, the opposite results were observed in LAPTM5-OE cells. Above all, these results indicated that LAPTM5 enhanced the progression and resistance to docetaxel in ER+ BC cells via activation of glutamine-mediated mTOR signaling.

Glutaminase inhibitor BPTES blocks the effect of LAPTM5 inhibition. To further elucidate the molecular mechanism of LAPTM5 in regulating ER+ BC, we treated blank

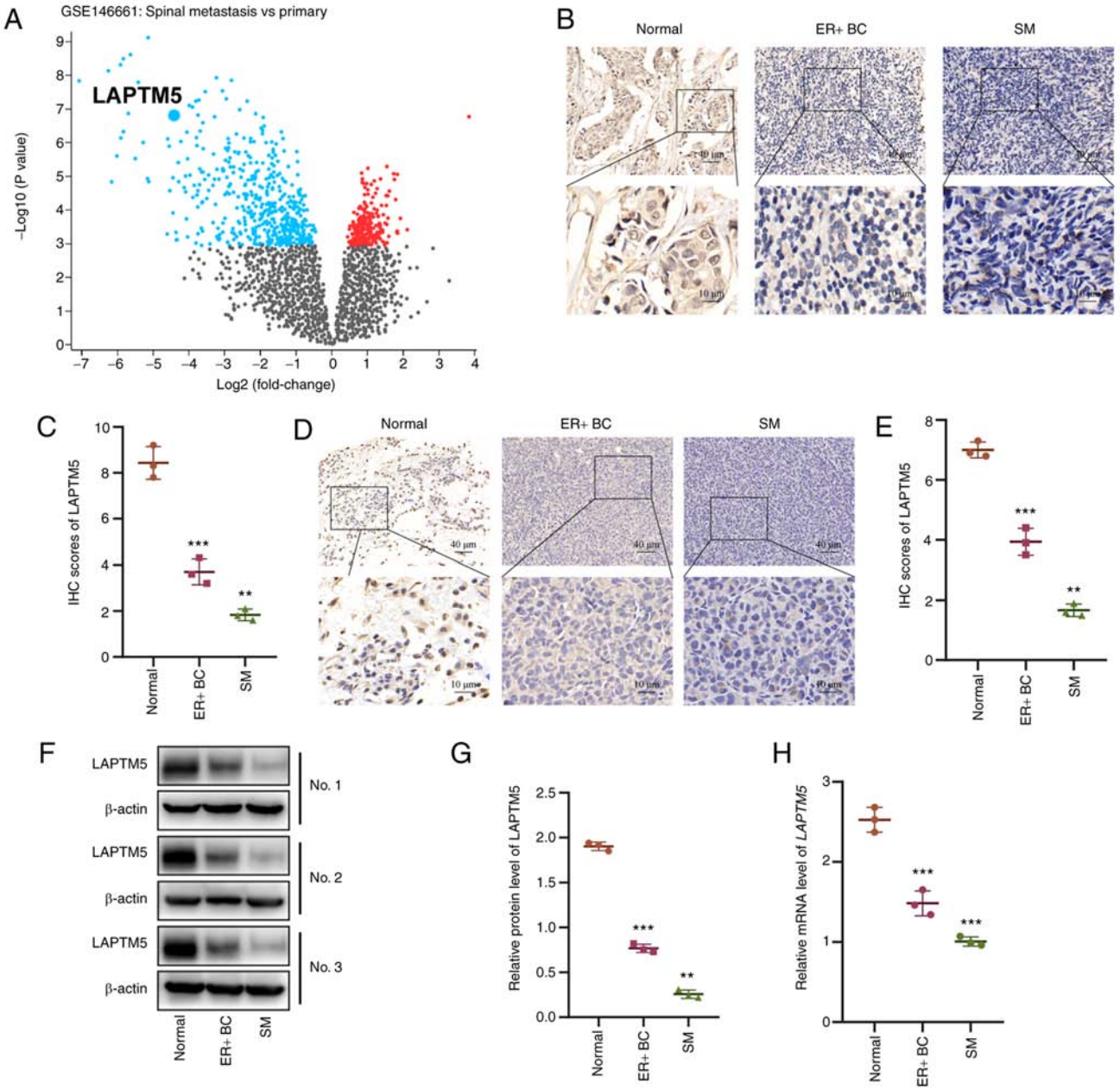

Figure 1. LAPTM5 expression is downregulated in ER+ BC, especially in SM tissue. (A) A volcano plot of the data (GSE14661) was obtained from GEO datasets. Each point represents a gene. Data points highlighted in blue represent genes that are downregulated in SM tissue. The volcano plot shows that LAPTM5 expression is significantly downregulated in SM tissue compared with that in primary ER+ BC tissue. (B) IHC staining of LAPTM5 in human ER+ BC tissue and its tumor-adjacent normal tissue and SM tissue. (C) Quantitative analysis of the IHC results of LAPTM5 in B. (D) IHC staining of LAPTM5 in mouse ER+ BC tissue, tumor-adjacent normal tissue and SM tissue. (E) Quantitative analysis of the IHC results of LAPTM5 in D. (F and G) Western blot and quantitative analysis of LAPTM5 in human ER+ BC tissue, tumor-adjacent normal tissue and SM tissue. (H) qPCR results of *laptm5* in mouse ER+ BC and SM tissue. **P<0.01 and ***P<0.001, compared to the tumor-adjacent normal tissue. LAPTM5, lysosomal protein transmembrane 5; ER+ BC, estrogen receptor-positive breast cancer; SM, spinal metastasis; IHC, immunohistochemistry.

or LAPTM5-sh3 cells with docetaxel, the glutaminase inhibitor BPTES, or both docetaxel and BPTES. As shown in Fig. 4A, after treatment with docetaxel alone, the activation of mTORC1 and the phosphorylation of its downstream factors S6K1 and 4EBP1 was suppressed in the blank ER+ BC cells by the chemotherapeutic drug. However, in LAPTM5-sh3 cells, Raptor, p-S6K1 and p-4EBP1 were even more highly activated than in cells without docetaxel treatment, indicating that downregulation of LAPTM5 expression decreased the chemosensitivity of ER+ BC cells. In contrast, the opposite results were observed in the LAPTM5-OE cells (Fig. 4L). Fig. 4B-K, M and N shows the quantitative analysis of the protein levels of Raptor, p-S6K1, and p-4EBP1 in the MCF-7 and T47D cell lines. In addition, BPTES treatment inhibited the activation of mTORC1 signaling in both blank and LAPTM5-sh3 cells with or without docetaxel treatment, demonstrating that glutamine-dependent mTORC1 signaling mediates the biological function of LAPTM5 in ER+ BC. Furthermore, GLS1 silencing (GLS1 sh1-3) significantly reversed the increased migration and proliferation of LAPTM5-sh3 ER+ BC cells (Fig. 5A-C). In addition, the activation of mTORC1 signaling after LAPTM5

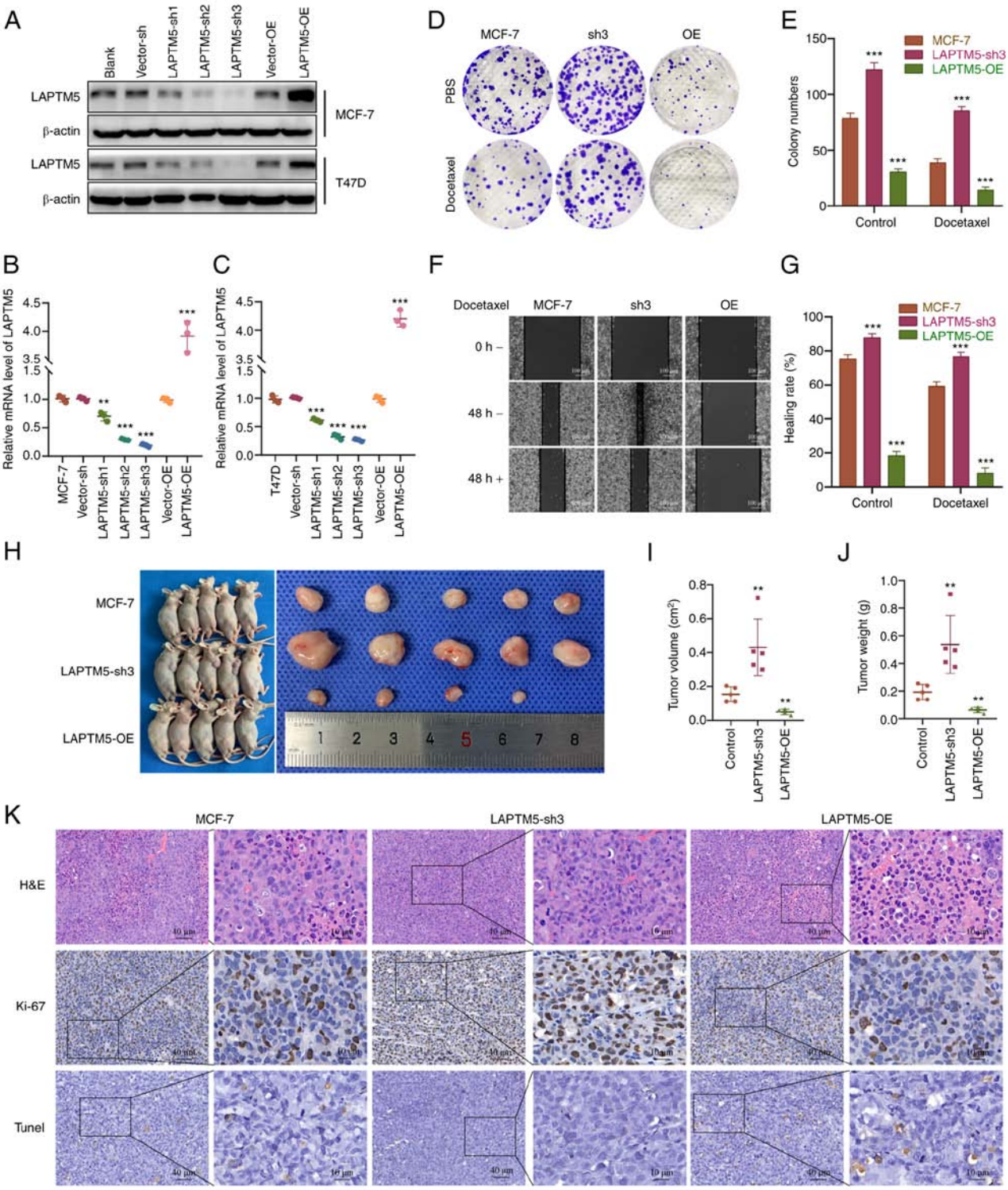

Figure 2. LAPTM5 is negatively associated with the proliferation and migration *in vitro* and tumorigenesis *in vivo* of ER+ BC cells under docetaxel treatment. (A) The establishment of LAPTM5-knockdown (sh1-3) or -overexpressing (OE) MCF-7 and T47D cell lines. The relative mRNA levels of *LAPTM5* in MCF-7 (B) and T47D (C) cells. **P<0.01 and ***P<0.001, compared with the blank MCF-7 and T47D cells. (D) Colony formation results of blank, LAPTM5-sh3 and LAPTM5-OE MCF-7 cells with or without docetaxel treatment. (E) Statistical analysis of the colony formation assay. ***P<0.001, compared with the blank MCF-7 cells. (F) The wound healing results of blank, LAPTM5-sh3 and LAPTM5-OE MCF-7 cells with or without docetaxel treatment. (G) Statistical analysis of the wound healing assay. ***P<0.001, compared with the blank MCF-7 cells. (H) Subcutaneous tumorigenesis of blank, LAPTM5-sh3 and LAPTM5-OE MCF-7 cells under docetaxel treatment. (I and J) Statistical analyses of tumor volume and weight. **P<0.01, compared with the mouse group inoculated with MCF-7 blank cells. (K) H&E, Ki-67 and TUNEL staining results of the above three groups. LAPTM5, lysosomal protein transmembrane 5; ER+ BC, estrogen receptor-positive breast cancer.

silencing was inhibited by downregulation of GLS1 expression (Fig. 5D and E). These results further confirmed that glutamine-induced mTOR signaling mediates the biological function of LAPTM5 in ER+ BC. Therefore, these data demonstrated that glutamine metabolism could be a therapeutic target for ER+ BC at the late stage.

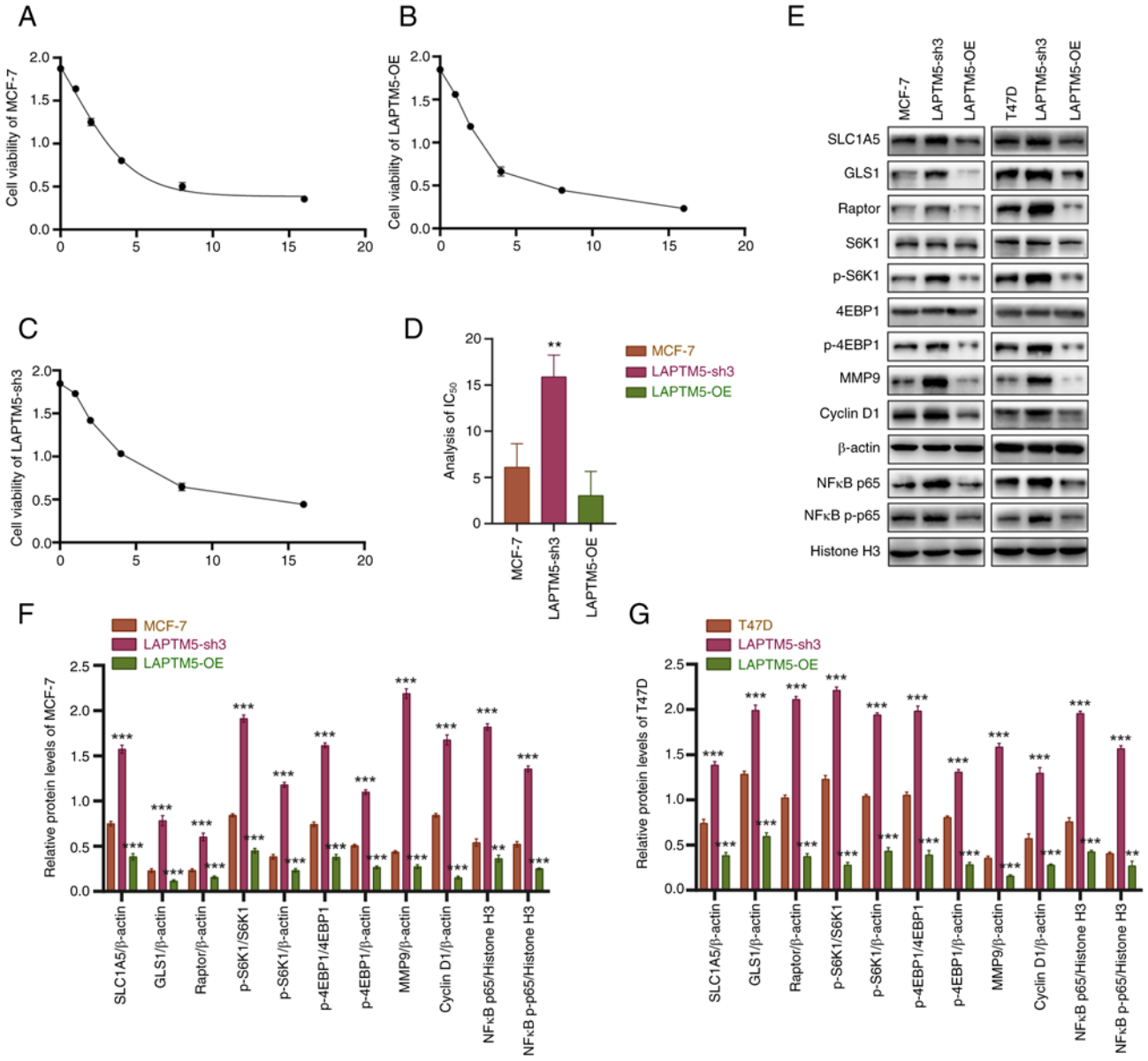

Figure 3. LAPTM5 enhances the resistance to docetaxel in ER+ BC cells via the activation of glutamine-mediated mTOR signaling. (A-C) Cell viability curves of blank (A), LAPTM5-sh3 (knockdown) (C) and LAPTM5-OE (overexpressing) MCF-7 (B) cells treated with 0, 1, 2, 4, 8, or 16 μM docetaxel for 24 h. (D) Statistical analysis of the half maximal inhibitory concentration (IC_{50}) values of the above three cell lines. **P<0.01, compared to the blank MCF-7 cells. (E) Protein expression and densitometric analysis results of key molecules of glutamine metabolism and mTOR signaling in blank, LAPTM5-sh3 and LAPTM5-OE MCF-7 and T47D cells. (F and G) Relative protein levels of LAPTM5 in the different MCF-7 (F) and T47D (G) cells. **P<0.01 and ***P<0.001, compared with the blank MCF-7 and T47D cells. LAPTM5, lysosomal protein transmembrane 5; ER$^+$ BC, estrogen receptor-positive breast cancer; SLC1A5, sodium-dependent neutral amino acid transporter type 2; GLS1, glutaminase 1; S6K1, ribosomal protein S6 kinase 1; 4EBP1, eukaryotic translation initiation factor 4E (eIF4E)-binding protein 1; MMP9, matrix metallopeptidase 9; nuclear factor κB, NFκB; p-, phosphorylated.

CX3CL1/CX3CR1 interaction mediates vertebrae-specific inhibition of LAPTM5. In our previous studies, CX3CL1/CX3CR1 was shown to be highly expressed in vertebrae and mediated SM in several types of cancer (25,33-35). However, the role of CX3CL1/CX3CR1 in the SM of ER$^+$ BC has not been fully elucidated. First, we demonstrated the high expression levels of CX3CR1 in the SM samples of ER$^+$ BC in both human patients and mouse models, while CX3CR1 expression was higher in the primary ER$^+$ BC tissue than that in the tumor-adjacent normal tissue (Fig. 6A-C). Preliminary experiments were conducted to determine the relationship between CX3CL1 and LAPTM5. When stimulated by CX3CL1, LAPTM5 was significantly inhibited in the ER$^+$ BC cells, while LAPTM5 inhibition was reversed after coculture with the CX3CR1-specific inhibitors JMS-17-2 and CX3CL1, indicating a negative regulatory effect of CX3CL1 on LAPTM5 expression (Fig. 6D). Then, blank and LAPTM5-OE cells were used to further confirm the relationship between CX3CL1/CX3CR1 and LAPTM5. As shown in Fig. 6E, CX3CL1 treatment significantly decreased LAPTM5 expression levels in both the blank and LAPTM5-OE cells, while JMS-17-2 blocked the inhibitory effect of CX3CL1 on LAPTM5. These results demonstrated that the CX3CL1/CX3CR1 interaction could reduce LAPTM5 expression, which may explain the lower expression of LAPTM5 in SM samples of ER$^+$ BC than that in primary tumor or normal

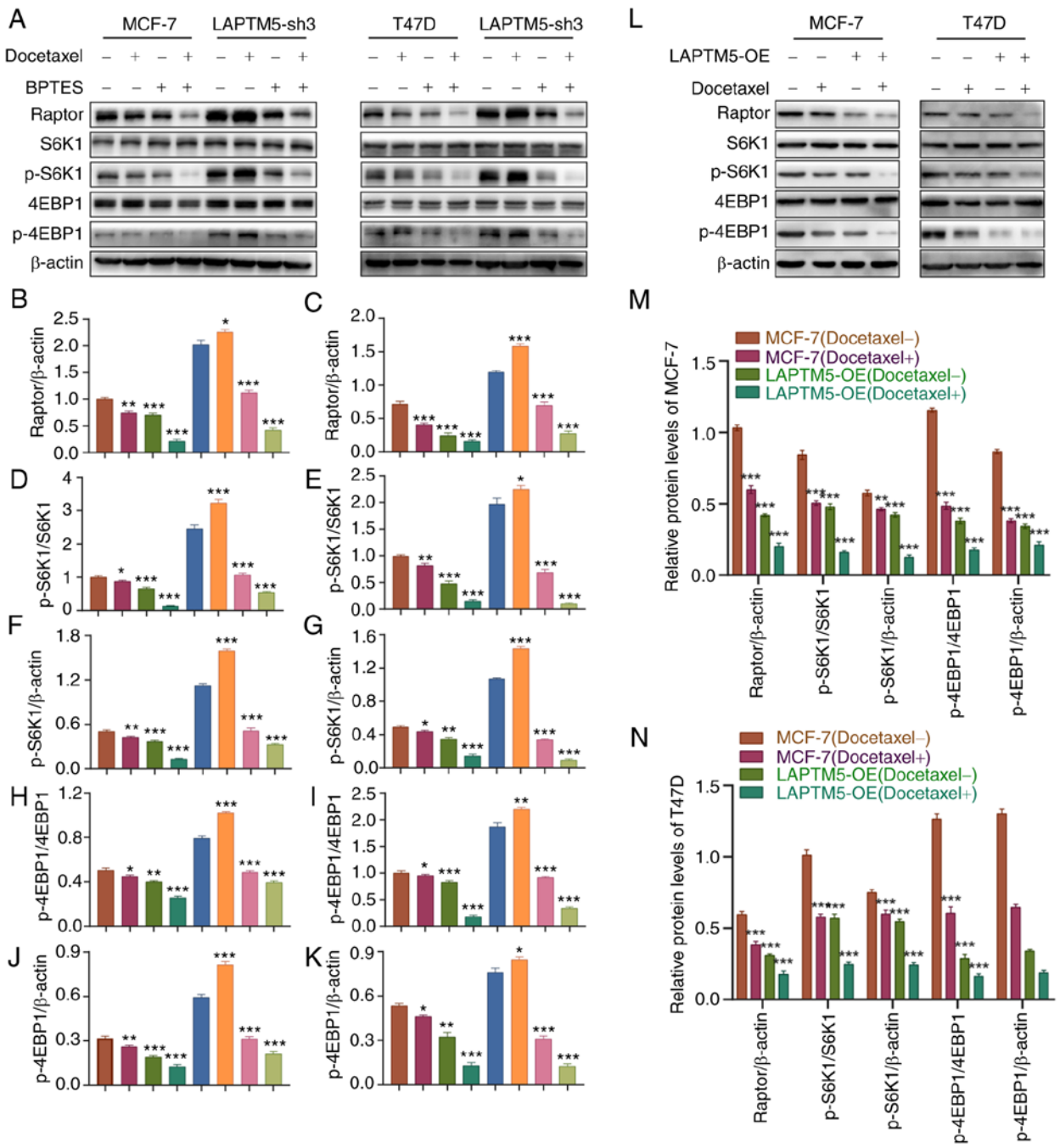

Figure 4. The glutaminase inhibitor BPTES reverses activation of mTOR signaling in LAPTM5-knockdown ER+ BC cells. (A) Protein expression of key molecules of glutamine metabolism and mTOR signaling in the blank and LAPTM5-sh3 (knockdown) MCF-7 and T47D cells when treated with docetaxel or the SLC1A5 inhibitor BPTES. (B-K) The relative protein expression of Raptor, p-S6K1, and p-4EBP1 in MCF-7 and T47D cells. (L) Protein expression of key molecules of glutamine metabolism and mTOR signaling in the blank and LAPTM5-OE (overexpessing) MCF-7 and T47D cells when treated with docetaxel. The relative protein expression of Raptor, p-S6K1, and p-4EBP1 in MCF-7 (M) and T47D (N) cells. *P<0.05, **P<0.01, and ***P<0.001, compared with the blank MCF-7 and T47D cells. LAPTM5, lysosomal protein transmembrane 5; ER+ BC, estrogen receptor-positive breast cancer; S6K1, ribosomal protein S6 kinase 1; 4EBP1, eukaryotic translation initiation factor 4E (eIF4E)-binding protein 1; p-, phosphorylated.

tissues. Furthermore, CX3CL1/CX3CR1-related signaling pathways were tested to reveal the mechanism by which high spinal CX3CL1/CX3CR1 levels influence the expression of LAPTM5. Among the various signaling pathways, PI3K/AKT signaling was most obviously involved, as both JMS-17-2 and the AKT-specific inhibitor MK-2206 reversed the activation of PI3K/AKT signaling and the subsequent inhibition of LAPTM5 (Fig. 6F). Collectively, these results demonstrated that a high expression level of CX3CL1/CX3CR1 in the spine facilitated SM in ER+ BC by inhibiting LAPTM5 expression to promote the growth, migration, and chemoresistance of cancer cells.

Blockade of CX3CL1/CX3CR1 or glutamine metabolism inhibits SM and enhances the chemosensitivity of ER+ BC. Finally, we detected the role of the CX3CL1/CX3CR1/LAPTM5/glutamine metabolic axis in the SM of ER+ BC and tested the potential therapeutic targets with an SM

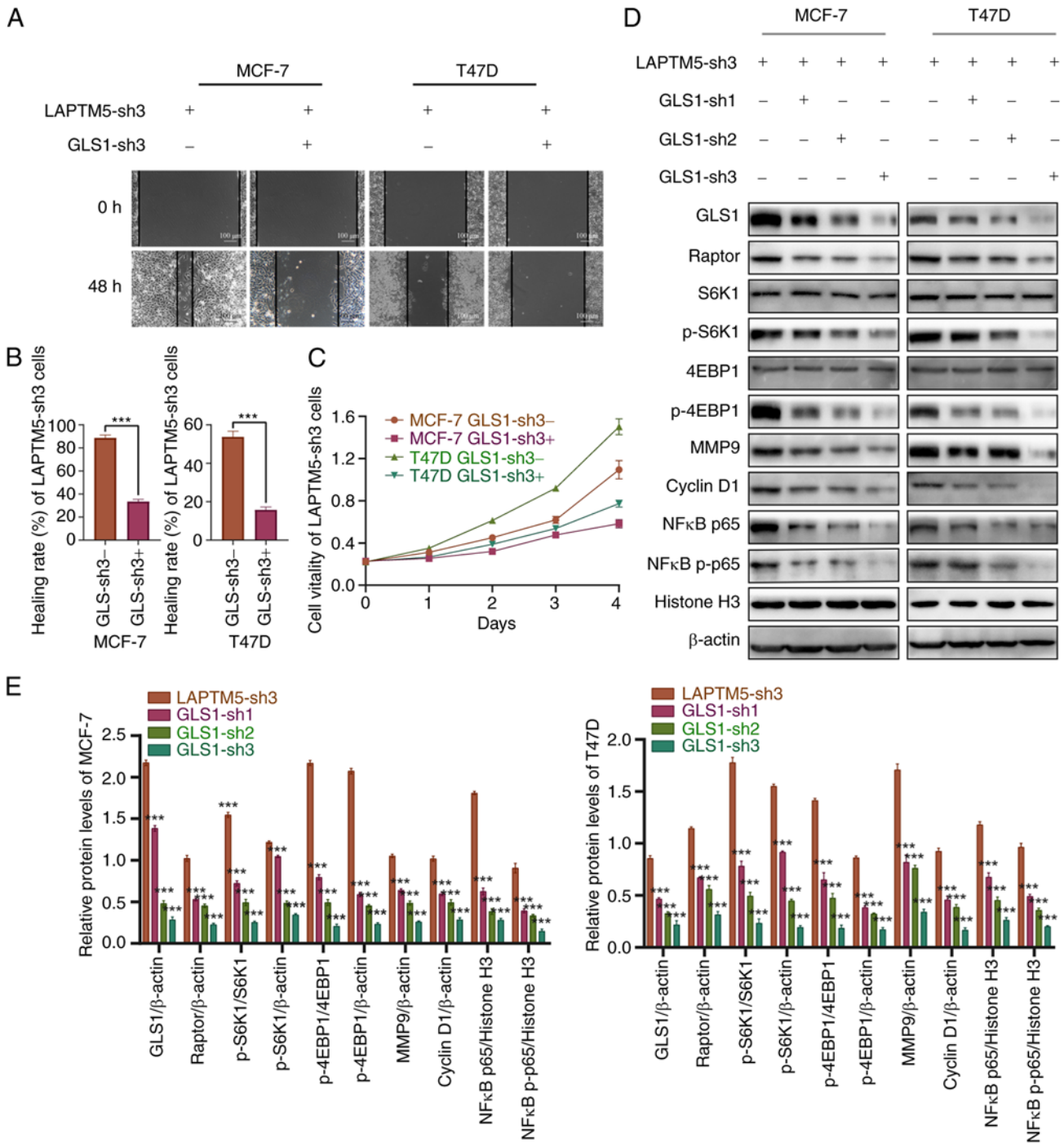

Figure 5. GLS1 silencing prevents increased proliferation and migration, as well as the activation of mTORC1 signaling of LAPTM5-sh3 cells. (A) The wound healing results of the LAPTM5-sh3 (knockdown) MCF-7 and T47D cells with or without GLS1 silencing. (B) Statistical analysis of the wound healing assay. ***P<0.001. (C) The CCK-8 results of the LAPTM5-sh3 MCF-7 and T47D cells with or without GLS1 silencing. (D and E) Protein expression (D) and densitometric analysis results (E) of key molecules of mTOR signaling in the GLS1-silenced LAPTM5-sh3 MCF-7 and T47D cells. LAPTM5, lysosomal protein transmembrane 5; GLS1, glutaminase 1; S6K1, ribosomal protein S6 kinase 1; 4EBP1, eukaryotic translation initiation factor 4E (eIF4E)-binding protein 1; MMP9, matrix metallopeptidase 9; nuclear factor κB, NFκB; p-, phosphorylated.

mouse model. As shown in Fig. 7A, the mouse model established with blank MCF-7 cells was set as the control group (a). The other groups were established with LAPTM5-sh3 cells and groups b-f were injected with saline (b), docetaxel (c), BPTES+docetaxel (d), JMS-17-2+docetaxel (e), and BPTES+JMS-17-2+docetaxel (f). One month after inoculation with cancer cells and injection of drugs, BLI and *ex vivo* tumor images visually showed the SM of ER$^+$ BC, as more SM was observed in group b, while docetaxel only slightly inhibited the SM of cancer cells (Figs. 7A and S5A). Moreover, both BPTES and JMS-17-2 improved the therapeutic effect of docetaxel, while co-injection of BPTES and JMS-17-2 improved chemosensitivity to the greatest extent. As shown in Fig. S5B and C, BPTES and JMS-17-2 treatment significantly delayed the occurrence of SM and prolonged the survival of the mice. Consistent with the above results, micro-CT was

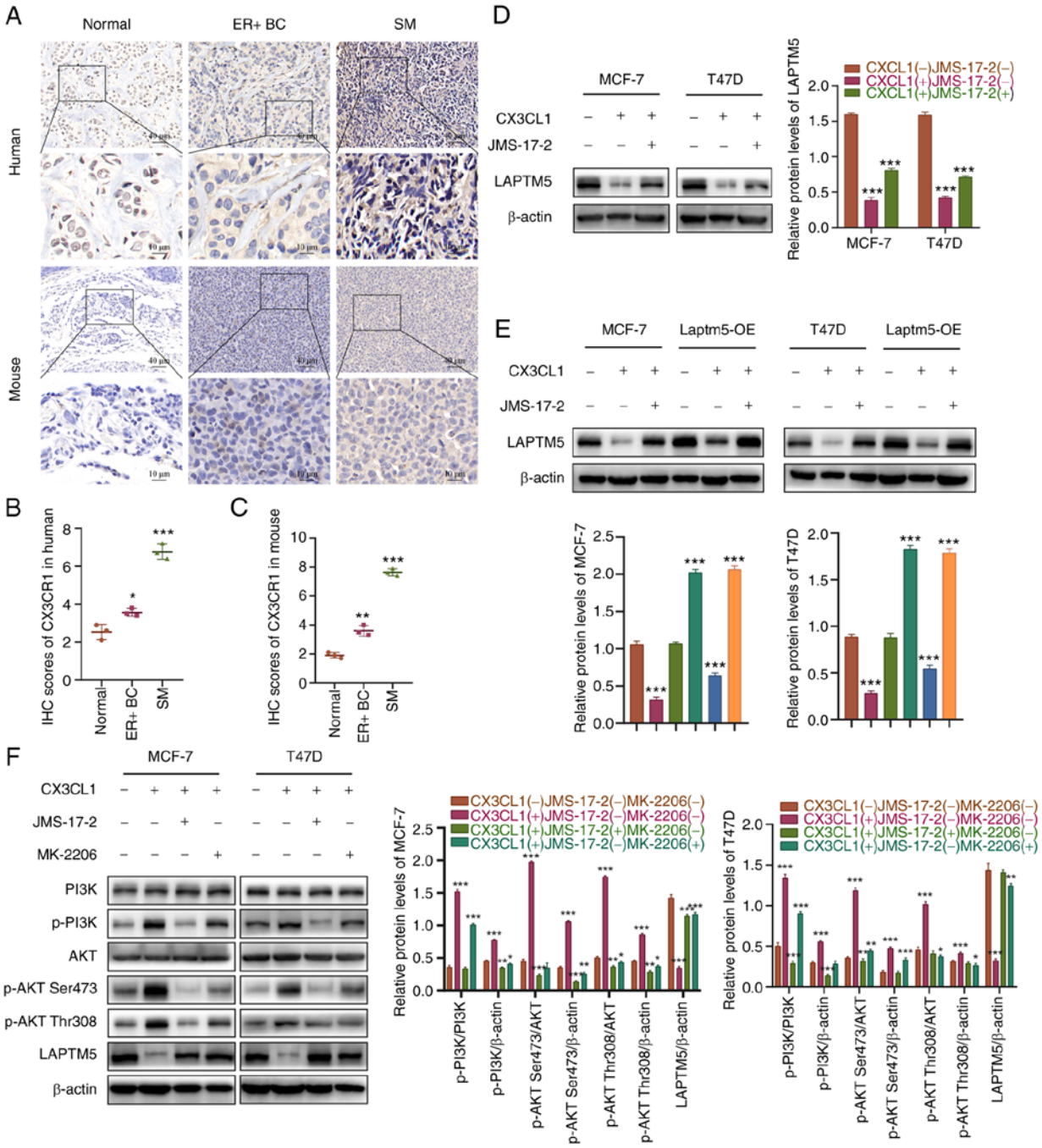

Figure 6. CX3CL1/CX3CR1 interaction mediates SM of ER+ BC cells by activating PI3K/AKT signaling to downregulate LAPTM5 expression. (A) IHC staining of CX3CR1 in ER+ BC tissue, tumor-adjacent normal tissue and SM tissue from patients and mouse models. (B and C) Quantitative analysis of the IHC results of CX3CR1. *P<0.05, **P<0.01, and ***P<0.001, compared to the normal tissues. (D) The protein level of LAPTM5 under CX3CL1 and/or the CX3CR1 inhibitor JMS-17-2 treatment. ***P<0.001, compared to untreated cells. (E) The protein level of LAPTM5 in blank and LAPTM5-OE (overexpressing) cells treated with CX3CL1 and/or the CX3CR1 inhibitor JMS-17-2. ***P<0.001, compared to untreated cells. (F) Activation of PI3K/AKT signaling and LAPTM5 expression under PBS, CX3CL1, CX3CL1+JMS-17-2, or CX3CL1+MK-2206 (AKT inhibitor) treatment. *P<0.05, **P<0.01, and ***P<0.001, compared with the untreated cells. LAPTM5, lysosomal protein transmembrane 5; ER+ BC, estrogen receptor-positive breast cancer; CX3CL1, C-X3-C motif chemokine ligand 1; CX3CR1, C-X3-C motif chemokine receptor 1; SM, spinal metastasis; p-, phosphorylated.

applied to observe bone destruction by cancer cells, and the results exhibited obvious lesions of the spine in groups a-c, while almost no lesions were found in group f (Fig. 7B). H&E staining showed similar results (Fig. 7C). IHC staining for CX3CR1, GLS1 and Raptor further confirmed that the inhibition of LAPTM5 promoted SM of ER+ BC and that blockade of glutamine metabolism and CX3CL1/CX3CR1 reversed the chemoresistance of LAPTM5-sh3 cells (Fig. 7A and D-F).

Discussion

The exact role of lysosomal protein transmembrane 5 (LAPTM5) in human estrogen receptor-positive (ER+) breast cancer (BC) has not been reported and is still unclear. Given that LAPTM5 was reported to suppress several types of solid tumors (12,13), our preliminary analysis indicated that LAPTM5 expression was significantly downregulated in spinal metastasis (SM)

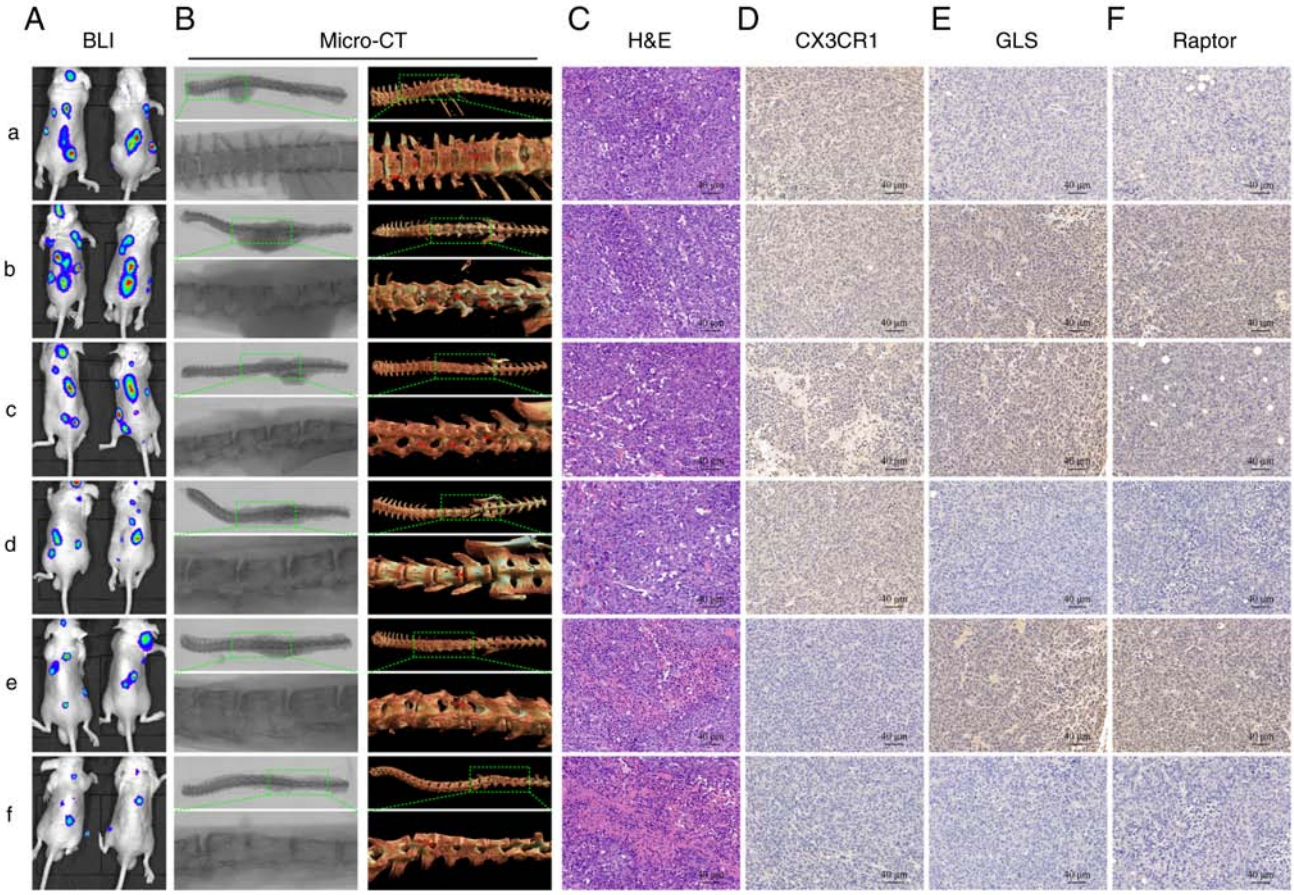

Figure 7. Blockade of CX3CL1/CX3CR1 and glutaminase inhibits SM and enhances the chemosensitivity of ER+ BC cells. (A) Representative bioluminescence imaging (BLI) imaging of each mouse group. (B) Representative micro-CT images of each group. (C) Hematoxylin and eosin (H&E) staining of each group. (D-F) Immunohistochemistry (IHC) staining for CX3CR1, GLS1, and Raptor in each group. Blank MCF-7 cells were used as the control group (a). The other groups were established with LAPTM5-sh3 (knockdown) cells, and groups (b-f) were injected with saline (b), docetaxel (c), BPTES+docetaxel (d), JMS-17-2+docetaxel (e), and BPTES+JMS-17-2+docetaxel (f). CX3CL1, C-X3-C motif chemokine ligand 1; CX3CR1, C-X3-C motif chemokine receptor 1; ER+ BC, estrogen receptor-positive breast cancer; SM, spinal metastasis; LAPTM5, lysosomal protein transmembrane 5; GLS1, glutaminase 1.

specimens of ER+ BC compared with its primary lesions as determined from the GEO dataset. The tumor-suppressive role of LAPTM5 in ER+ BC was verified by detecting LAPTM5 expression in ER+ BC tissue and its tumor-adjacent normal tissue and SM samples from patients and mouse models. Moreover, these data indicated that decreased LAPTM5 expression was related to the SM of ER+ BC. In addition, we also observed SM in mice injected with LAPTM5-overexpressing (OE) MCF-7 cells, but no obvious SM could be found via bioluminescence imaging (BLI) and micro-CT (data not shown). This study mainly discussed the downregulation of LAPTM5 and its involvement in the promotion of SM of ER+ BC and how to prevent spinal metastasis via blocking downstream molecules of LAPTM5; therefore, only results of LAPTM5-sh3 knockdown groups were exhibited in Fig. 7. At the late stage of ER+ BC, the degree of malignancy of cancer cells in SM is much higher than that in the primary site, which is characterized by faster growth and migration and enhanced resistance to chemotherapies (7,8). These results prompted us to determine the exact role and mechanism of LAPTM5 in ER+ BC and how LAPTM5 mediates the development of SM.

As a tumor suppressor, LAPTM5 mainly has a negative regulatory effect on receptor-mediated signaling in T cells or B cells (36,37). Although the direct impact of LAPTM5 on cancer cells has attracted much attention in recent years, data concerning ER+ BC have not been reported. In our preliminary experiments, we investigated the tumorigenic ability of LAPTM5-sh3, LAPTM5-OE, and blank MCF-7 cells. The results showed that LAPTM5 silencing significantly enhanced the *in vivo* tumorigenesis of ER+ BC in the absence of docetaxel (data not shown). Interestingly, our results demonstrated that decreased LAPTM5 expression strongly enhanced the growth and migration rates, as well as resistance to chemotherapeutic drugs, of ER+ BC. After we demonstrated the role of LAPTM5 in ER+ BC, the underlying mechanism was also investigated. As the gene set enrichment analysis indicated that nutrient metabolism is closely related to LAPTM5 expression, we detected the degree of glutamine metabolism of the blank ER+ BC cells compared with the LAPTM5-sh or LAPTM5-OE cells. Here, for the first time, we demonstrated that glutamine metabolism was regulated by LAPTM5 and mediated the role of LAPTM5 in ER+ BC.

Glutamine promotes the growth and migration of cancer cells, as it provides a nitrogen source for synthesizing nucleotides and nonessential amino acids and a carbon source for the tricarboxylic acid cycle and fatty acid synthesis (38,39). Recently, glutamine transporters were found to be overexpressed in ER+ BC, indicating the critical role and

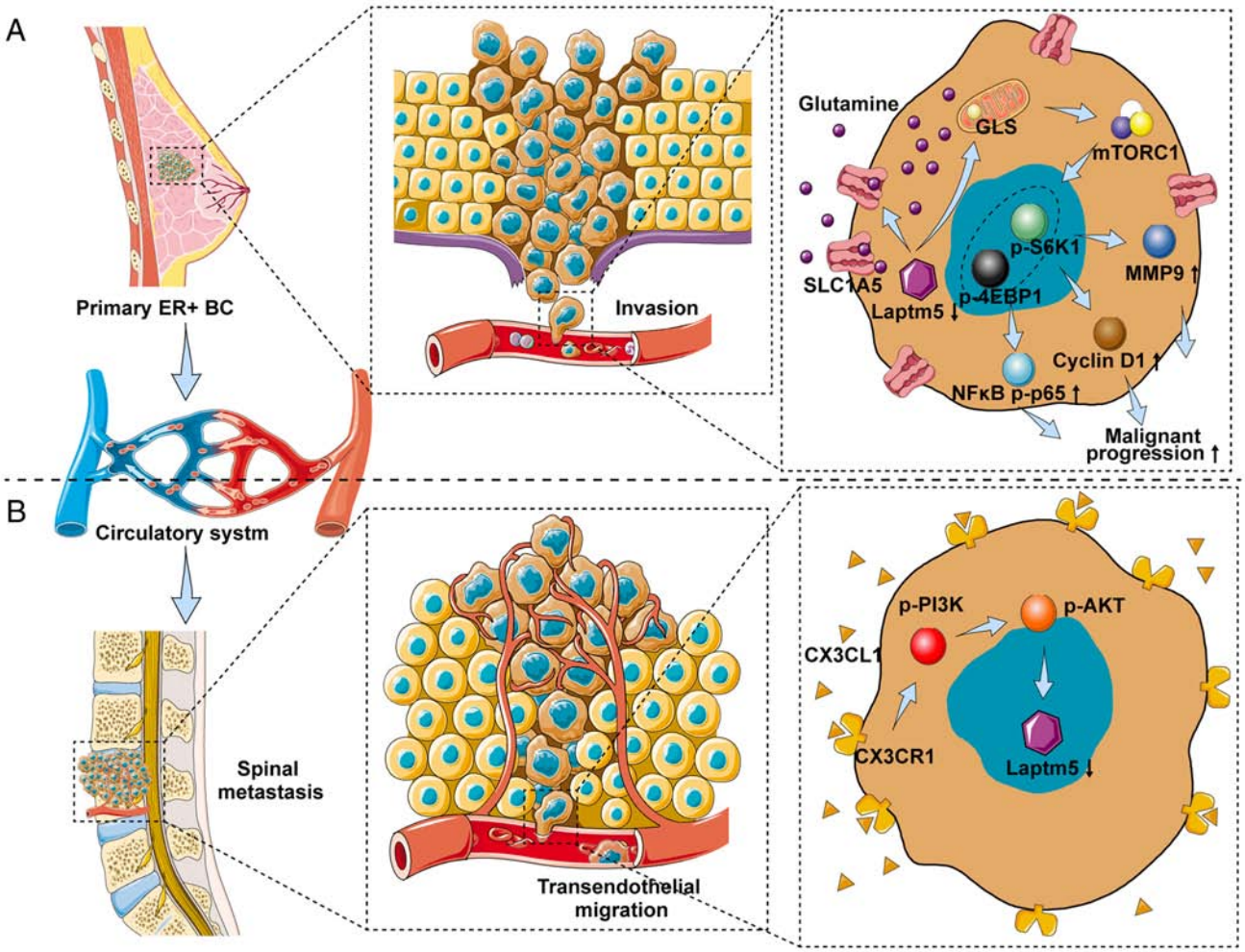

Figure 8. Schematic depicting the role of LAPTM5 in regulating the malignant progression and SM of ER+ BC. (A) LAPTM5 downregulation promotes the proliferation, migration, and chemoresistance of ER+ BC cells by activating glutamine-mediated mTOR signaling. (B) CX3CL1/CX3CR1 interaction mediates the vertebrae-specific inhibition of LAPTM5 and the SM of ER+ BC via PI3K/AKT signaling. LAPTM5, lysosomal protein transmembrane 5; ER+ BC, estrogen receptor-positive breast cancer; CX3CL1, C-X3-C motif chemokine ligand 1; CX3CR1, C-X3-C motif chemokine receptor 1; SM, spinal metastasis; GLS, glutaminase; S6K1, ribosomal protein S6 kinase 1; 4EBP1, eukaryotic translation initiation factor 4E (eIF4E)-binding protein 1; MMP9, matrix metallopeptidase 9; nuclear factor κB, NFκB.

potential mechanism of glutamine metabolism in ER+ BC (40). Sodium-dependent neutral amino acid transporter type 2 (SLC1A5) and glutaminase 1 (GLS1) are two major upstream regulators in the glutamine metabolic process (18,41). SLC1A5, also known as ASCT2, is a neutral amino acid transporter located on the cell surface that mediates the uptake of glutamine (18). GLS1 can convert glutamine to glutamate and then fuel the tricarboxylic acid cycle (41). The expression of both SLC1A5 and GLS1 was upregulated when LAPTM5 was inhibited, suggesting that LAPTM5 inhibition activates glutamine metabolism. Glutamine, as the primary source of carbon and nitrogen for maintaining vital activities of cancer cells, has been reported to facilitate poor progression of BC (17). Therefore, oncogenic alteration of LAPTM5 could reprogram glutamine metabolism to regulate cancer cells.

Many signaling pathways are activated by reprogrammed glutamine metabolism. Among them, mTORC1 was reported to be one of the main downstream pathways of glutamine metabolism (42,43). Studies have shown that molecules that influence amino acid transportation or glutamine consumption are involved in controlling mTOR recruitment and activation (42). mTORC1, the complex composed of mTOR, Raptor, and mLST8, is activated by amino acids, including glutamine, and energy metabolism, which regulates proliferation, migration, chemoresistance, and other mTORC1-mediated processes (43,44). After the formation of mTORC1, activated mTORC1 phosphorylates S6K1 and 4EBP1 to promote the expression of metalloproteinase (MMP)9 and cyclin D1 and activate NFκB signaling, explaining the enhanced migration, proliferation, and chemoresistance of ER+ BC (45). MMP9 is involved in degrading the extracellular matrix in the tissue remodeling process to enhance the migration and invasion of cancer cells, while cyclin D1 plays an important role in driving cell proliferation and promoting chemoresistance in BC (46,47). Moreover, NFκB renders BC cells resistant to chemotherapies, and its inhibitors are considered promising anti-BC drugs (48). As mentioned earlier, we demonstrated that LAPTM5 inhibition could activate SLC1A5 and GLS1 to enhance glutamine metabolism, which resulted in activation of mTORC1. In contrast, the SLC1A5 inhibitor BPTES reversed the activation of mTORC1 by downregulating LAPTM5 expression,

further confirming that glutamine-dependent mTOR activation mediates the role of LAPTM5 in ER+ BC.

Emerging evidence has shown that the interaction and activation of CX3CL1/CX3CR1 facilitate the SM of circulating tumor cells (25,33-35). Here, for the first time, we demonstrated that CX3CL1/CX3CR1 interaction downregulated LAPTM5 expression, and the inhibition of the latter was proven to be closely related to the enhanced proliferation, migration, and chemoresistance of ER+ BC. We inferred that when circulating ER+ BC cells reaches the spine, the abundant CX3CL1 interacts with CX3CR1 on the surface of cancer cells to downregulate LAPTM5 expression and then promotes the viability of cancer cells even under chemotherapy treatment, facilitating the invasion of ER+ BC in the spine. Furthermore, we found that CX3CL1 stimulation downregulated LAPTM5 expression via PI3K/AKT signaling, which was reported to be downstream of the CX3CL1/CX3CR1 interaction (Fig. 8). Therefore, we believe that a high concentration of CX3CL1 mediates spine-specific inhibition of LAPTM5 to facilitate SM of ER+ BC. Finally, with an SM mouse model, we verified the tumor-suppressive role of LAPTM5 in ER+ BC and confirmed the SM-specific targeting effect of the CX3CL1/CX3CR1/LAPTM5/glutamine axis.

In summary, we demonstrated that downregulation of LAPTM5 expression could regulate glutamine metabolism through SLC1A5 and GLS1 to activate mTOR signaling and promote the proliferation, migration, and chemoresistance of ER+ BC. In addition, a high level of CX3CL1 in the spine inhibited LAPTM5 expression through interaction with CX3CR1, indicating that the CX3CL1/CX3CR1/LAPTM5/glutamine axis mediates the SM of ER+ BC. Therefore, the CX3CL1/CX3CR1/LAPTM5/glutamine metabolic axis may be a prospective therapeutic target for ER+ BC and its SM, suggesting that upregulation of LAPTM5 expression or blockade of its downstream signaling could alleviate the malignancy of ER+ BC.

Acknowledgements

Not applicable.

Funding

This work was supported by the National Natural Science Foundation of China (nos. 82172738, 81972508 and 81772855).

Availability of data and materials

The datasets used and/or analyzed during the present study are available from the corresponding author on reasonable request.

Authors' contributions

QM and JD designed the experiments. LZ, LJ and HLia collected the samples. QM, LZ, HLia, AH and HZ conducted the experiments and acquired the data. JZ, XZ, HLin, LJ and XL analyzed the data and confirmed the integrity of the data. QM and JD wrote the manuscript. All authors read and approved the manuscript and agree to be accountable for all aspects of the research in ensuring that the accuracy or integrity of any part of the work are appropriately investigated and resolved.

Ethics approval and consent to participate

The animal experiments were approved (approval no. 2020-032, 2020.04.06) by the Animal Ethics Committee of Zhongshan Hospital, Fudan University (Shanghai, China).

Patient consent for publication

Not applicable.

Competing interests

The authors declare that they have no competing interests.

References

1. Akram M, Iqbal M, Daniyal M and Khan AU: Awareness and current knowledge of breast cancer. Biol Res 50: 33, 2017.
2. Chen W, Zheng R, Baade PD, Zhang S, Zeng H, Bray F, Jemal A, Yu XQ and He J: Cancer statistics in China, 2015. CA Cancer J Clin 66: 115-132, 2016.
3. Liang Y, Zhang H, Song X and Yang Q: Metastatic heterogeneity of breast cancer: Molecular mechanism and potential therapeutic targets. Semin Cancer Biol 60: 14-27, 2020.
4. Scully OJ, Bay BH, Yip G and Yu Y: Breast cancer metastasis. Cancer Genomics Proteomics 9: 311-320, 2012.
5. Turner NC, Neven P, Loibl S and Andre F: Advances in the treatment of advanced oestrogen-receptor-positive breast cancer. Lancet 389: 2403-2414, 2017.
6. Chen WZ, Shen JF, Zhou Y, Chen XY, Liu JM and Liu ZL: Clinical characteristics and risk factors for developing bone metastases in patients with breast cancer. Sci Rep 7: 11325, 2017.
7. Ma RY, Zhang H, Li XF, Zhang CB, Selli C, Tagliavini G, Lam AD, Prost S, Sims AH, Hu HY, *et al*: Monocyte-derived macrophages promote breast cancer bone metastasis outgrowth. J Exp Med 217: e20191820, 2020.
8. Tahara RK, Brewer TM, Theriault RL and Ueno NT: Bone metastasis of breast cancer. Adv Exp Med Biol 1152: 105-129, 2019.
9. Glowacka WK, Alberts P, Ouchida R, Wang JY and Rotin D: LAPTM5 protein is a positive regulator of proinflammatory signaling pathways in macrophages. J Biol Chem 287: 27691-27702, 2012.
10. Liu X, Shang X, Li J and Zhang S: The prognosis and immune checkpoint blockade efficacy prediction of tumor-infiltrating immune cells in lung cancer. Front Cell Dev Biol 9: 707143, 2021.
11. Zhang L, Zhang M, Chen X, He Y, Chen R, Zhang J, Huang J, Ouyang C and Shi G: Identification of the tubulointerstitial infiltrating immune cell landscape and immune marker related molecular patterns in lupus nephritis using bioinformatics analysis. Ann Transl Med 8: 1596, 2020.
12. Berberich A, Bartels F, Tang Z, Knoll M, Pusch S, Hucke N, Kessler T, Dong Z, Wiestler B, Winkler F, *et al*: LAPTM5-CD40 crosstalk in glioblastoma invasion and temozolomide resistance. Front Oncol 10: 747, 2020.
13. Nuylan M, Kawano T, Inazawa J and Inoue J: Down-regulation of LAPTM5 in human cancer cells. Oncotarget 7: 28320-28328, 2016.
14. Mossmann D, Park S and Hall MN: mTOR signalling and cellular metabolism are mutual determinants in cancer. Nat Rev Cancer 18: 744-757, 2018.
15. Vander Heiden MG and DeBerardinis RJ: Understanding the intersections between metabolism and cancer biology. Cell 168: 657-669, 2017.
16. Reinfeld BI, Madden MZ, Wolf MM, Chytil A, Bader JE, Patterson AR, Sugiura A, Cohen AS, Ali A, Do BT, *et al*: Cell-programmed nutrient partitioning in the tumour microenvironment. Nature 593: 282-288, 2021.
17. Cha YJ, Kim ES and Koo JS: Amino acid transporters and glutamine metabolism in breast cancer. Int J Mol Sci 19: 907, 2018.

18. van Geldermalsen M, Wang Q, Nagarajah R, Marshall AD, Thoeng A, Gao D, Ritchie W, Feng Y, Bailey CG, Deng N, *et al*: ASCT2/SLC1A5 controls glutamine uptake and tumour growth in triple-negative basal-like breast cancer. Oncogene 35: 3201-3208, 2016.
19. Kodama M, Oshikawa K, Shimizu H, Yoshioka S, Takahashi M, Izumi Y, Bamba T, Tateishi C, Tomonaga T, Matsumoto M and Nakayama KI: A shift in glutamine nitrogen metabolism contributes to the malignant progression of cancer. Nat Commun 11: 1320, 2020.
20. Feng M, Xiong G, Cao Z, Yang G, Zheng S, Qiu J, You L, Zheng L, Zhang T and Zhao Y: LAT2 regulates glutamine-dependent mTOR activation to promote glycolysis and chemoresistance in pancreatic cancer. J Exp Clin Cancer Res 37: 274, 2018.
21. Ramapriyan R, Caetano MS, Barsoumian HB, Mafra ACP, Zambalde EP, Menon H, Tsouko E, Welsh JW and Cortez MA: Altered cancer metabolism in mechanisms of immunotherapy resistance. Pharmacol Ther 195: 162-171, 2019.
22. Korbecki J, Simińska D, Kojder K, Grochans S, Gutowska I, Chlubek D and Baranowska-Bosiacka I: Fractalkine/CX3CL1 in neoplastic processes. Int J Mol Sci 21: 3723, 2020.
23. Liang Y, Yi L, Liu P, Jiang L, Wang H, Hu A, Sun C and Dong J: CX3CL1 involves in breast cancer metastasizing to the spine via the Src/FAK signaling pathway. J Cancer 9: 3603-3612, 2018.
24. Jiang G, Wang H, Huang D, Wu Y, Ding W, Zhou Q, Ding Q, Zhang N, Na R and Xu K: The clinical implications and molecular mechanism of CX3CL1 expression in urothelial bladder cancer. Front Oncol 11: 752860, 2021.
25. Wang K, Jiang L, Hu A, Sun C, Zhou L, Huang Y, Chen Q, Dong J, Zhou X and Zhang F: Vertebral-specific activation of the CX3CL1/ICAM-1 signaling network mediates non-small-cell lung cancer spinal metastasis by engaging tumor cell-vertebral bone marrow endothelial cell interactions. Theranostics 11: 4770-4789, 2021.
26. Huang da W, Sherman BT and Lempicki RA: Systematic and integrative analysis of large gene lists using DAVID bioinformatics resources. Nat Protoc 4: 44-57, 2009.
27. Huang da W, Sherman BT and Lempicki RA: Bioinformatics enrichment tools: Paths toward the comprehensive functional analysis of large gene lists. Nucleic Acids Res 37: 1-13, 2009.
28. Lichter JG, Carruth E, Mitchell C, Barth AS, Aiba T, Kass DA, Tomaselli GF, Bridge JH and Sachse FB: Remodeling of the sarcomeric cytoskeleton in cardiac ventricular myocytes during heart failure and after cardiac resynchronization therapy. J Mol Cell Cardiol 72: 186-195, 2014.
29. Livak KJ and Schmittgen TD: Analysis of relative gene expression data using real-time quantitative PCR and the 2(-Delta Delta C(T)) method. Methods 25: 402-408, 2001.
30. Xiang Y, Stine ZE, Xia J, Lu Y, O'Connor RS, Altman BJ, Hsieh AL, Gouw AM, Thomas AG, Gao P, *et al*: Targeted inhibition of tumor-specific glutaminase diminishes cell-autonomous tumorigenesis. J Clin Invest 125: 2293-2306, 2015.
31. Shen F, Zhang Y, Jernigan DL, Feng X, Yan J, Garcia FU, Meucci O, Salvino JM and Fatatis A: Novel small-molecule CX3CR1 antagonist impairs metastatic seeding and colonization of breast cancer cells. Mol Cancer Res 14: 518-527, 2016.
32. Montaudon E, Nikitorowicz-Buniak J, Sourd L, Morisset L, El Botty R, Huguet L, Dahmani A, Painsec P, Nemati F, Vacher S, *et al*: PLK1 inhibition exhibits strong anti-tumoral activity in CCND1-driven breast cancer metastases with acquired palbociclib resistance. Nat Commun 11: 4053, 2020.
33. Liu W, Jiang L, Bian C, Liang Y, Xing R, Yishakea M and Dong J: Role of CX3CL1 in diseases. Arch Immunol Ther Exp (Warsz) 64: 371-383, 2016.
34. Sun C, Hu A, Wang S, Tian B, Jiang L, Liang Y, Wang H and Dong J: ADAM17-regulated CX3CL1 expression produced by bone marrow endothelial cells promotes spinal metastasis from hepatocellular carcinoma. Int J Oncol 57: 249-263, 2020.
35. Yi L, Liang Y, Zhao Q, Wang H and Dong J: CX3CL1 induces vertebral microvascular barrier dysfunction via the Src/P115-RhoGEF/ROCK signaling pathway. Front Cell Neurosci 14: 96, 2020.
36. Tu J, Kuang Z, Xie X, Wu S, Wu T and Chen S: Prognostic and predictive value of a mRNA signature in peripheral T-cell lymphomas: A mRNA expression analysis. J Cell Mol Med 25: 84-95, 2021.
37. Zouali M: Transcriptional and metabolic pre-B cell receptor-mediated checkpoints: Implications for autoimmune diseases. Mol Immunol 62: 315-320, 2014.
38. Cory JG and Cory AH: Critical roles of glutamine as nitrogen donors in purine and pyrimidine nucleotide synthesis: Asparaginase treatment in childhood acute lymphoblastic leukemia. In Vivo 20: 587-589, 2006.
39. Metallo CM, Gameiro PA, Bell EL, Mattaini KR, Yang J, Hiller K, Jewell CM, Johnson ZR, Irvine DJ, Guarente L, *et al*: Reductive glutamine metabolism by IDH1 mediates lipogenesis under hypoxia. Nature 481: 380-384, 2011.
40. Karunakaran S, Ramachandran S, Coothankandaswamy V, Elangovan S, Babu E, Periyasamy-Thandavan S, Gurav A, Gnanaprakasam JP, Singh N, Schoenlein PV, *et al*: SLC6A14 (ATB0,+) protein, a highly concentrative and broad specific amino acid transporter, is a novel and effective drug target for treatment of estrogen receptor-positive breast cancer. J Biol Chem 286: 31830-31838, 2011.
41. Matés JM, Campos-Sandoval JA, Santos-Jiménez JL and Márquez J: Dysregulation of glutaminase and glutamine synthetase in cancer. Cancer Lett 467: 29-39, 2019.
42. Jewell JL, Kim YC, Russell RC, Yu FX, Park HW, Plouffe SW, Tagliabracci VS and Guan KL: Metabolism. Differential regulation of mTORC1 by leucine and glutamine. Science 347: 194-198, 2015.
43. Meng D, Yang Q, Wang H, Melick CH, Navlani R, Frank AR and Jewell JL: Glutamine and asparagine activate mTORC1 independently of Rag GTPases. J Biol Chem 295: 2890-2899, 2020.
44. Csibi A, Fendt SM, Li C, Poulogiannis G, Choo AY, Chapski DJ, Jeong SM, Dempsey JM, Parkhitko A, Morrison T, *et al*: The mTORC1 pathway stimulates glutamine metabolism and cell proliferation by repressing SIRT4. Cell 153: 840-854, 2013.
45. Hua H, Kong Q, Zhang H, Wang J, Luo T and Jiang Y: Targeting mTOR for cancer therapy. J Hematol Oncol 12: 71, 2019.
46. Zhen Y, Liu J, Huang Y, Wang Y, Li W and Wu J: miR-133b inhibits cell growth, migration, and invasion by targeting MMP9 in non-small cell lung cancer. Oncol Res 25: 1109-1116, 2017.
47. Shi Q, Li Y, Li S, Jin L, Lai H, Wu Y, Cai Z, Zhu M, Li Q, Li Y, *et al*: LncRNA DILA1 inhibits cyclin D1 degradation and contributes to tamoxifen resistance in breast cancer. Nat Commun 11: 5513, 2020.
48. Ling J and Kumar R: Crosstalk between NFkB and glucocorticoid signaling: A potential target of breast cancer therapy. Cancer Lett 322: 119-126, 2012.